

SUPPLEMENTARY DATA

Supplementary Material for: Saturated Fat is More Metabolically Harmful for the Human Liver than Unsaturated Fat or Simple Sugars

Panu K. Luukkonen^{1,2}, Sanja Sädevirta^{1,2}, You Zhou^{1,3}, Brandon Kayser⁴, Ashfaq Ali⁵, Linda Ahonen⁵, Susanna Lallukka^{1,2}, Véronique Pelloux⁴, Melania Gaggini⁶, Ching Jian⁷, Antti Hakkarainen⁸, Nina Lundbom⁸, Helena Gylling², Anne Salonen⁷, Matej Orešič^{5,9,10}, Tuulia Hyötyläinen^{5,11}, Marju Orho-Melander¹², Aila Rissanen¹³, Amalia Gastaldelli⁶, Karine Clément^{4,14}, Leanne Hodson¹⁵, Hannele Yki-Järvinen^{1,2,16}

¹Minerva Foundation Institute for Medical Research, Helsinki, Finland; ²Department of Medicine, University of Helsinki and Helsinki University Central Hospital, Helsinki, Finland; ³Systems Immunity University Research Institute and Division of Infection and Immunity, School of Medicine, Cardiff University, Cardiff, United Kingdom; ⁴Sorbonne Universités, INSERM, UMRS 1166, Nutriomics team, ICAN, F-75013, Paris, France; ⁵Steno Diabetes Center, Gentofte, Denmark; ⁶Institute of Clinical Physiology, CNR, Pisa, Italy; ⁷Immunobiology Research Program, Department of Bacteriology and Immunology, University of Helsinki; ⁸Helsinki Medical Imaging Centre, Radiology, Helsinki University Hospital and University of Helsinki; ⁹School of Medical Sciences, Örebro University, Örebro, Sweden; ¹⁰Turku Centre for Biotechnology, University of Turku and Åbo Akademi University, Turku, Finland; ¹¹Department of Chemistry, Örebro University, Örebro, Sweden; ¹²Lund University, Malmö, Sweden; ¹³Obesity Research Unit, Department of Psychiatry, Helsinki University Central Hospital; ¹⁴Assistance Publique-Hôpitaux de Paris (AP-HP), Pitié-Salpêtrière Hospital, Nutrition Department F-75013, Paris, France; ¹⁵Oxford Centre for Diabetes, Endocrinology and Metabolism, University of Oxford, Oxford, UK; ¹⁶Corresponding Author

Table of contents

Adipose tissue transcriptome	2
Gut microbiota	3
DNL methodology	4
FA composition of VLDL-TG	4
References	5
Figure S1	6
Figure S2	7
Figure S3	8
Figure S4	9
Figure S5	10
Figure S6	11
Table S1	12
Table S2	13
Table S3	14

SUPPLEMENTARY DATA

Adipose tissue transcriptome

In the beginning of the study, after indirect calorimetry, a needle aspiration biopsy from abdominal subcutaneous adipose tissue was obtained under 1% lidocaine anesthesia and immediately frozen in liquid nitrogen and stored at -80°C until analysis. Total RNA was isolated using the RNeasy Lipid Tissue Mini Kit (Qiagen, Valencia, CA).

Bioinformatics. The Illumina HumanHT12v4 microarray chips (Illumina, San Diego, CA) were annotated using the IlluminaHumanv4.db from Bioconductor. A standard non-specific filtering approach was used to extract genes most likely to be expressed in the tissue and to ultimately limit the number of tests to genes of interest. Specifically, probes without annotation to a gene were removed, and if multiple probes matched to a gene, only the probe with the highest interquartile range across samples was included. Finally, only genes with inter-quartile range greater than the median of all genes were included. KEGG pathways were downloaded from the Molecular Signatures Database (<http://software.broadinstitute.org/gsea/msigdb/collections.jsp#C2>). To limit the number of tests to pathways of interest, unrelated pathways were removed e.g. Huntington's disease.

Statistical analysis. The pre/post comparisons within each diet were computed using LIMMA (1). Specifically, the two factors (time and diet) were converted into a single factor with 6 levels, and after running the full model, contrast tests between levels of interest were performed (e.g. Diet 1-Pre vs Diet 1-Post). The model was analyzed as a multi-level model to account for repeated measures. Array-quality weights were estimated and included in the model. Details of the LIMMA procedure can be found in the comprehensive manual (2).

For the reporter features analysis (3), \log_2 fold-change and unadjusted p-values from the LIMMA analysis were used as input. Statistical significance was determined from the null distribution and gene sets were limited to those with more than 3 genes and no more than 200. Otherwise, default parameters were used. Distinctly up- and down-regulated pathways were used to determine pathway enrichment in the specific direction. P-values were adjusted to the Benjamini-Hochberg false discovery rate.

SUPPLEMENTARY DATA

Gut microbiota

Bacterial DNA was extracted from fecal samples using mechanical cell lysis that efficiently extracts bacterial community DNA as previously described (4). Illumina MiSeq paired-end sequencing of the hypervariable V3-V4 regions of the 16S rRNA gene was performed according to the manual from Illumina except that the libraries were prepared with single-step PCR, i.e. by amplifying the 16S rRNA gene fragment together with barcoded primers, the latter adapted from Kozich et al (5). The multiplex PCR reaction is comprised of 1 ng/ul template, 1X Phusion® Master Mix (ThermoFisher, F-531L), 0.25 uM V3-V4 locus specific primers and 0.375 uM dual-index barcodes. The PCR was run under the following settings: 98 °C for 30 s, 27 cycles of 98 °C for 10 s, 62 °C for 30 s, 72 °C for 15 s and finally 10 min at 72 °C, where after the samples were stored at 4 °C. The size of the PCR product was expected to be ~640 base pairs (bp) and verified on a Bioanalyzer DNA 1000 chip (Agilent Technology, Santa Clara, CA, USA). The PCR clean-up was performed with AMPure XP beads (Beckman Coulter, Copenhagen, Denmark) and confirmation of the right size of the target was performed on a Bioanalyzer DNA 1000 chip (Agilent Technology, CA, USA). The pooled libraries were sequenced at the sequencing unit of the Institute for Molecular Medicine Finland (FIMM), Helsinki, Finland with an Illumina MiSeq instrument using paired end 2 × 300 bp reads and a MiSeq v3 reagent kit with 5% PhiX as spike-in.

Sequencing data preprocessing, analysis and statistics

The forward reads were truncated to length of 150 bases with `mare's "ProcessReads"` command. We used default settings for minimum quality score and maximum expected errors. Reads with prevalence below 0.01% were removed. Chimera removal and dereplication of the reads was done using USEARCH8 (6). Truncated, filtered and dereplicated reads were annotated using the Silva database (7). The median read count per sample after preprocessing was 68797 (range 296 –148 604). The data analysis was done without rarefaction or transformations utilizing statistical and visualization tools included in the `mare`-package (8). The number of reads was used as an offset in all statistical models. Community dissimilarity was estimated with principal coordinates analysis (PCoA) using Bray-Curtis dissimilarity as the distance measure. PCoA was calculated with `capscale` function of R package `vegan` and Bray-Curtis dissimilarities with function `vegdist` of the same package (9). Permutational multivariate analysis of variance using distance matrices was performed with `adonis` function in package `vegan` to calculate the relative contribution of different factors in the microbiota variation. Taxonomic richness was estimated as the number of observed OTUs after clustering the reads to operational taxonomic units (OTUs) using USEARCH8. Comparison of the abundance of bacterial genera between two time points in each intervention group was performed using generalized linear mixed models within "`GroupTest`" function of the

SUPPLEMENTARY DATA

mare package using subject as the random factor. This function uses the glmmADMB package (generalized linear mixed models built on AD Model Builder) of R software on background and assumes negative binomial distribution of abundance.

DNL methodology

Fasting DNL was assessed based on the incorporation of deuterium from $^2\text{H}_2\text{O}$ in plasma water (Finnigan GasBench-II, ThermoFisher Scientific, UK) into VLDL-TG palmitate using gas chromatography/mass spectrometry (GC/MS) with monitoring ions with mass-to-charge ratios (m/z) of 270 (M+0) and 271 (M+1) (10).

For the calculation of DNL in VLDL-TG using the mass isotopomer distributions, the maximum number of deuterium molecules synthesized from plasma palmitate was assumed to be 22 (11). When constant enrichment in the precursor pool (plasma water) was obtained, F was the enrichment of palmitate synthesized during the time between the loading dose of $^2\text{H}_2\text{O}$ and the collection time. When isotopic equilibrium in the product pool (palmitate) was obtained, F was constant. $F = \text{plasma palmitate enrichment} / (22 \times \text{plasma deuterium enrichment})$. The percentage of *de novo* lipogenesis (%DNL) was calculated by multiplying F by 100%. Absolute DNL was calculated by multiplying %DNL and the concentration of TG in VLDL (12).

Consistently with a number of previous studies (10, 12-18), we used deuterated water with less than 24 hour loading for measurements of DNL. If the labelling period was longer, it is likely that we would have found higher rates of DNL. However, then it would have been also more challenging to account for differences in the recirculation of labeled fatty acids. A limitation of measuring DNL after an overnight fast only, is that we were unable to assess the synthesis of other fatty acids from DNL such as C16:1n-7 and C18:0 as done by Wilke et al. (Diabetologia 2009) as the labeling period (~12 h) was not long enough.

Although we have anecdotal evidence that 3 weeks is long enough to clear the majority of labeled lipid products from the first study on the day before each of the metabolic study days, a blood sample was taken for measurement of background enrichment of ^2H in plasma water and VLDL-TG palmitate for measurement of DNL. Therefore we were able to account for any differences in plasma water and VLDL-TG for the second visit. Regarding other labeled precursors that may have been generated from the $^2\text{H}_2\text{O}$ administered at baseline, we did not measure labeling of ^2H -FFA palmitate in this study, as we have in previous studies found it to be minimal.

FA composition of VLDL-TG

VLDL was isolated by ultracentrifugation as described (19). Total lipids were extracted (20) and FA methyl esters (FAMES) prepared from TG as described (21). Separation and quantification (expressed as mol%) of FAMES was achieved on a HP6890 GC (Agilent Technologies, Stockport, UK) with flame ionisation detection.

SUPPLEMENTARY DATA

REFERENCES

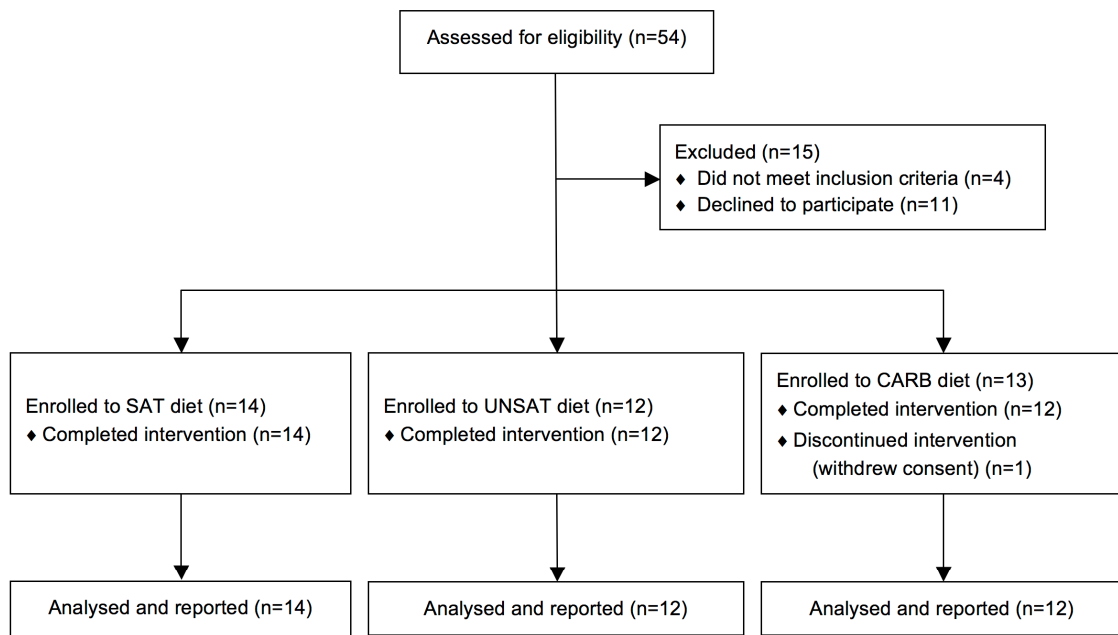
1. Smyth GK: Linear models and empirical bayes methods for assessing differential expression in microarray experiments. *Stat Appl Genet Mol Biol* 2004
2. Smyth GK, Ritchie M, Thorne N, Wettenhall J, Shi... W: *Limma: Linear Models for Microarray and RNA-Seq Data User's Guide*. Citeseer 2002
3. Väre L, Nielsen J, Nookaew I: Enriching the gene set analysis of genome-wide data by incorporating directionality of gene expression and combining statistical hypotheses and methods. *Nucleic Acids Res* 41:4378-4391, 2013
4. Salonen A, Nikkila J, Jalanka-Tuovinen J, Immonen O, Rajilic-Stojanovic M, Kekkonen RA, et al. (2010). Comparative analysis of fecal DNA extraction methods with phylogenetic microarray: effective recovery of bacterial and archaeal DNA using mechanical cell lysis. *J Microbiol Methods*. 81(2):127-34.
5. Kozich JJ, Westcott SL, Baxter NT, Highlander SK, Schloss PD. (2013). Development of a dual-index sequencing strategy and curation pipeline for analyzing amplicon sequence data on the MiSeq Illumina sequencing platform. *Appl Environ Microbiol*. 79(17):5112-20.
6. Edgar RC. (2010). Search and clustering orders of magnitude faster than BLAST. *Bioinformatics*. 26(19):2460-1.
7. Quast C, Pruesse E, Yilmaz P, Gerken J, Schweer T, Yarza P, et al. (2012). The SILVA ribosomal RNA gene database project: improved data processing and web-based tools. *Nucleic Acids Res*. gks1219.
8. Korpela K. (2016). *mare: Microbiota Analysis in R Easily*. R package version 10" 23-Apr-2016.
9. Oksanen JFGB, R. Kindt, P. Legendre, P.R. Minchin, R.B. O'Hara, G.L. Simpson, P. Solymos, M.H.H. Stevens, H.Wagner. (2011). Package 'vegan' version 2.0-2.
10. Semple RK, Sleigh A, Murgatroyd PR, et al. (2009). Postreceptor insulin resistance contributes to human dyslipidemia and hepatic steatosis. *J Clin Invest*. 119(2):315-22.
11. Diraison F, Pachiardi C, Beylot M. Measuring lipogenesis and cholesterol synthesis in humans with deuterated water: use of simple gas chromatographic/mass spectrometric techniques. *J Mass Spectrom*. 1997;32(1):81-6.
12. Santoro N, Caprio S, Pierpont B, et al. (2015). Hepatic De Novo Lipogenesis in Obese Youth Is Modulated by a Common Variant in the GCKR Gene. *J Clin Endocrinol Metab*. 100(8):E1125-32.
13. Matikainen N, Adiels M, Söderlund S, Stenabb S, Ahola T, Hakkarainen A, Borén J, Taskinen MR. Hepatic lipogenesis and a marker of hepatic lipid oxidation, predict postprandial responses of triglyceride-rich lipoproteins. *Obesity (Silver Spring)*. 2014;22(8):1854-9.
14. Lambert JE, Ramos-Roman MA, Browning JD, Parks EJ. Increased de novo lipogenesis is a distinct characteristic of individuals with nonalcoholic fatty liver disease. *Gastroenterology*. 2014;146(3):726-35.
15. Pramfalk C, Pavlides M, Banerjee R, McNeil CA, Neubauer S, Karpe F, Hodson L. Sex-Specific Differences in Hepatic Fat Oxidation and Synthesis May Explain the Higher Propensity for NAFLD in Men. *J Clin Endocrinol Metab*. 2015;100(12):4425-33.
16. Pramfalk C, Pavlides M, Banerjee R, McNeil CA, Neubauer S, Karpe F, Hodson L. Fasting Plasma Insulin Concentrations Are Associated With Changes in Hepatic Fatty Acid Synthesis and Partitioning Prior to Changes in Liver Fat Content in Healthy Adults. *Diabetes*. 2016;65(7):1858-67.
17. Hodson L, Banerjee R, Rial B, Arlt W, Adiels M, Boren J, Marinou K, Fisher C, Mostad IL, Stratton IM, Barrett PH, Chan DC, Watts GF, Harnden K, Karpe F, Fielding BA. Menopausal Status and Abdominal Obesity Are Significant Determinants of Hepatic Lipid Metabolism in Women. *J Am Heart Assoc*. 2015;4(10):e002258.
18. Hazlehurst JM, Oprescu AI, Nikolaou N, Di Guida R, Grinbergs AE, Davies NP, Flintham RB, Armstrong MJ, Taylor AE, Hughes BA, Yu J, Hodson L, Dunn WB, Tomlinson JW. Dual-5 α -Reductase Inhibition Promotes Hepatic Lipid Accumulation in Man. *J Clin Endocrinol Metab*. 2016;101(1):103-13.
19. Sevastianova K, Santos A, Kotronen A, Hakkarainen A, Makkonen J, Silander K, Peltonen M, Romeo S, Lundbom J, Lundbom N, Olkkonen VM, Gylling H, Fielding BA, Rissanen A, Yki-Järvinen H. Effect of short-term carbohydrate overfeeding and long-term weight loss on liver fat in overweight humans. *Am J Clin Nutr*. 2012;96(4):727-34.

SUPPLEMENTARY DATA

20. Folch J, Lees M, Sloane Stanley GH. (1957). A simple method for the isolation and purification of total lipides from animal tissues. *J Biol Chem.* 226(1): 497-509.

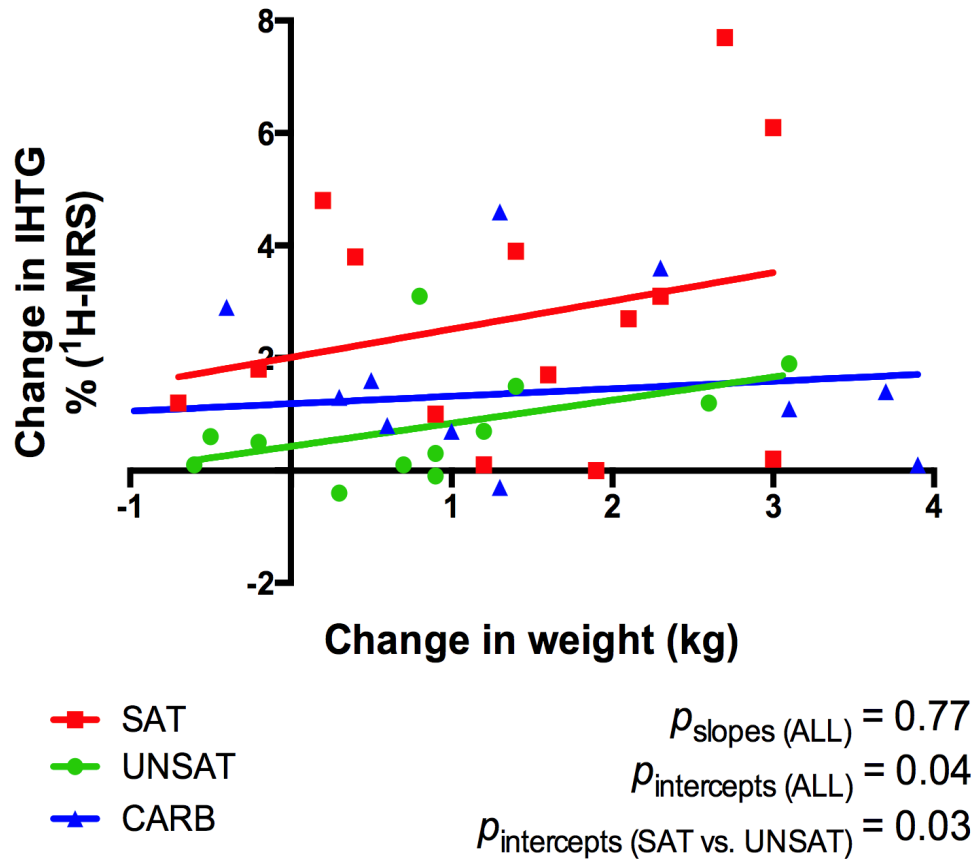
21. Heath RB, Karpe F, Milne RW, et al. (2003). Selective partitioning of dietary fatty acids into the VLDL TG pool in the early postprandial period. *J Lipid Res.* 44(11):2065-72.

Supplementary Figure S1. Study flow chart. A total of 54 subjects were assessed for eligibility, 39 of whom were considered eligible. One subject withdrew from the study. Data were collected and analyzed on 14 subjects enrolled to the SAT diet, 12 subjects enrolled to the UNSAT diet, and 12 subjects enrolled to the CARB diet.



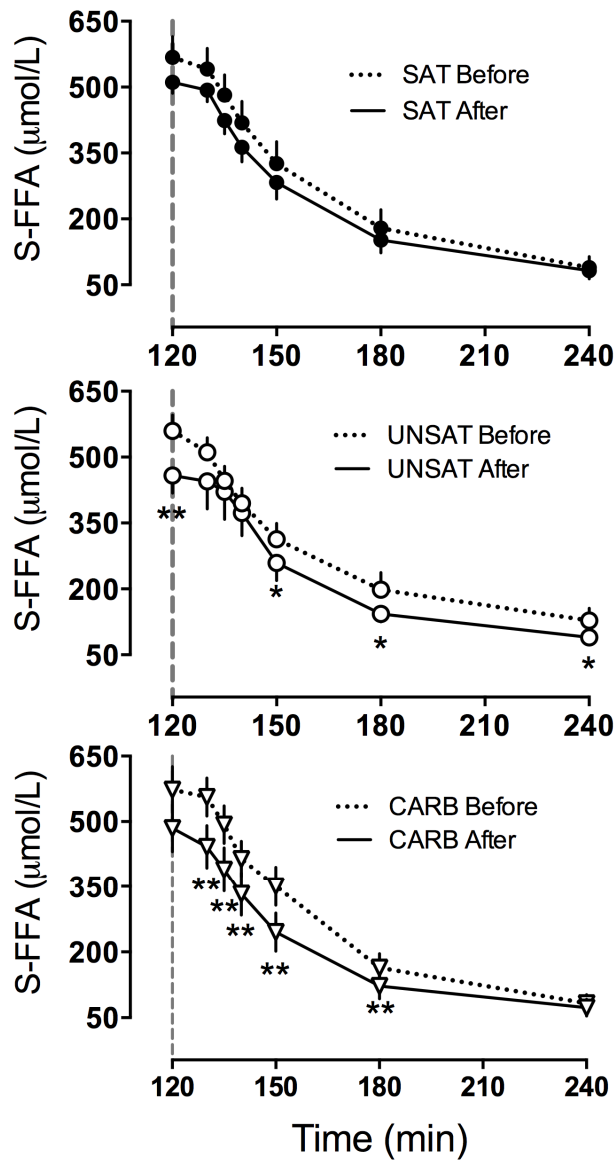
SUPPLEMENTARY DATA

Supplementary Figure S2. Linear regression between change in intrahepatic triglycerides (IHTG) and change in weight in the diet groups. The y-axis denotes the change in IHTG after versus before overfeeding as %-units determined by proton magnetic resonance spectroscopy (^1H -MRS). The x-axis denotes the change in body weight in kilograms after versus before overfeeding. Red symbols and line = saturated fat (SAT) group; green symbols and line = unsaturated fat (UNSAT) group; blue symbols and line = simple sugar (CARB) group.



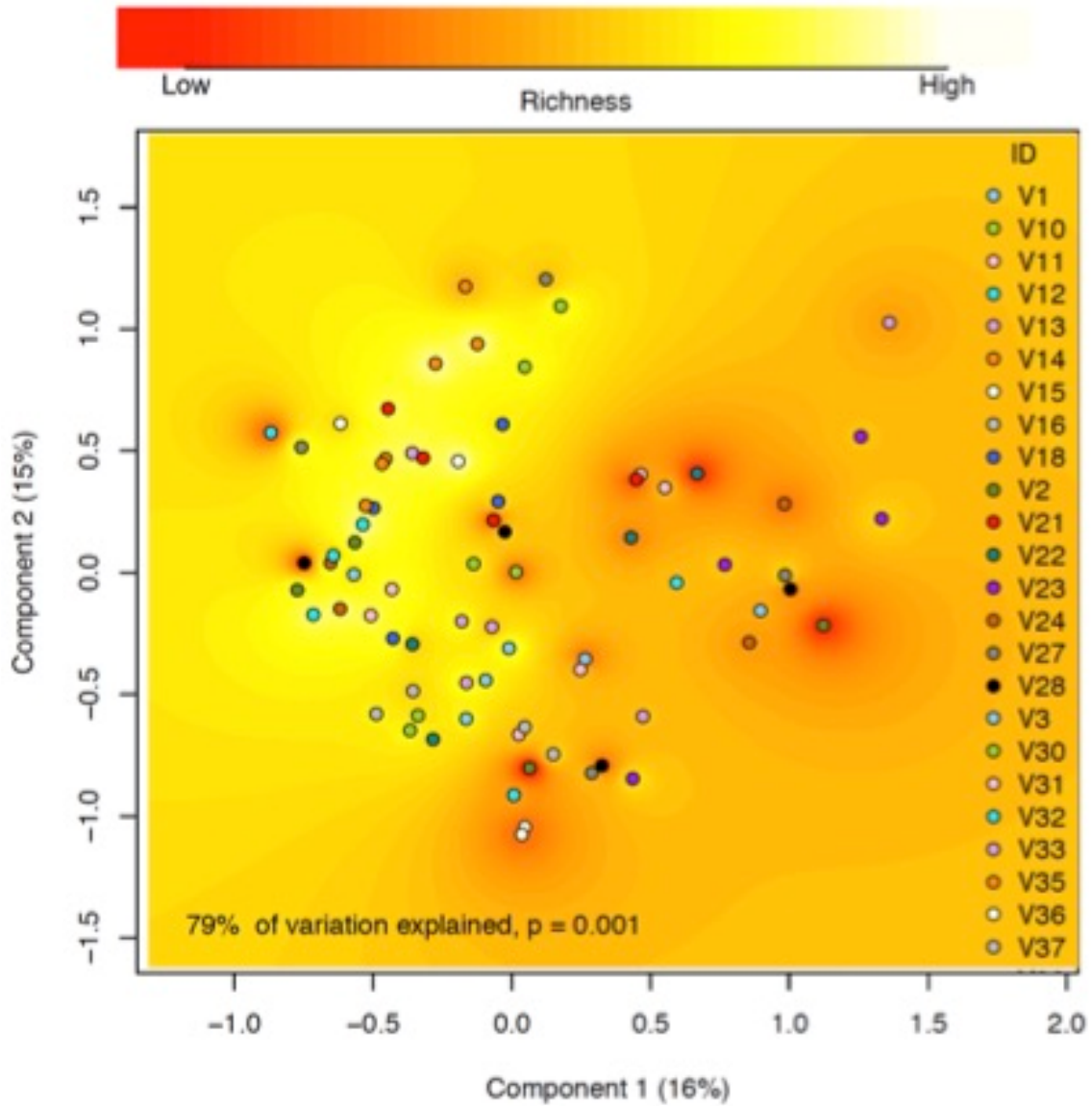
SUPPLEMENTARY DATA

Supplementary Figure S3. Serum free fatty acid (FFA) concentrations during euglycemic hyperinsulinemic clamp before and after the overfeeding. SAT = saturated fat (panel on the top), UNSAT = unsaturated fat (panel in the middle), CARB = simple sugar group (panel on the bottom). The x-axes denote serum FFA concentration and the y-axes time from the beginning of the study (euglycemic hyperinsulinemic clamp was started at 120 minutes). * $p < 0.05$, ** $p < 0.01$.



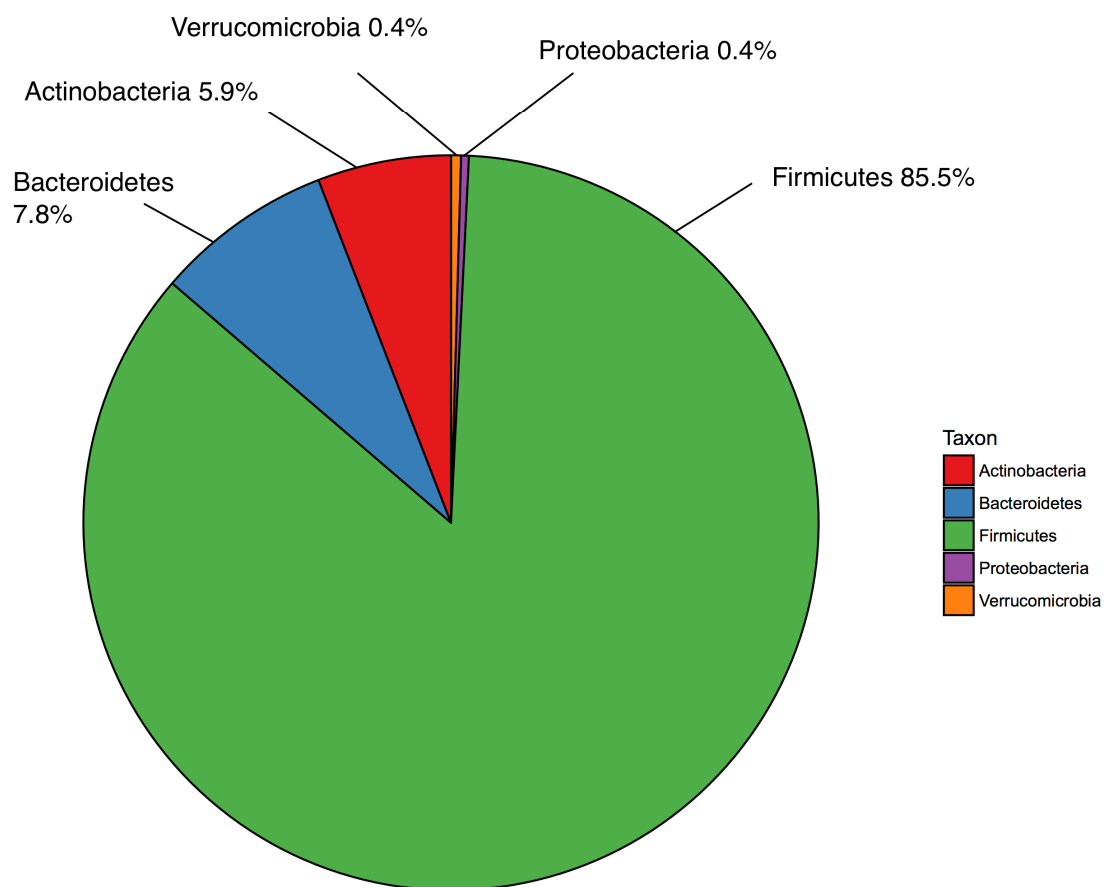
SUPPLEMENTARY DATA

Supplementary Figure S4. Principal coordinates analysis (PCoA) plot based on Bray-Curtis dissimilarity of all the microbiota samples, coloured according to the subject. The background colour indicates microbiota richness. Permutational multivariate analysis of variance was used to calculate the explanatory power of the subject.



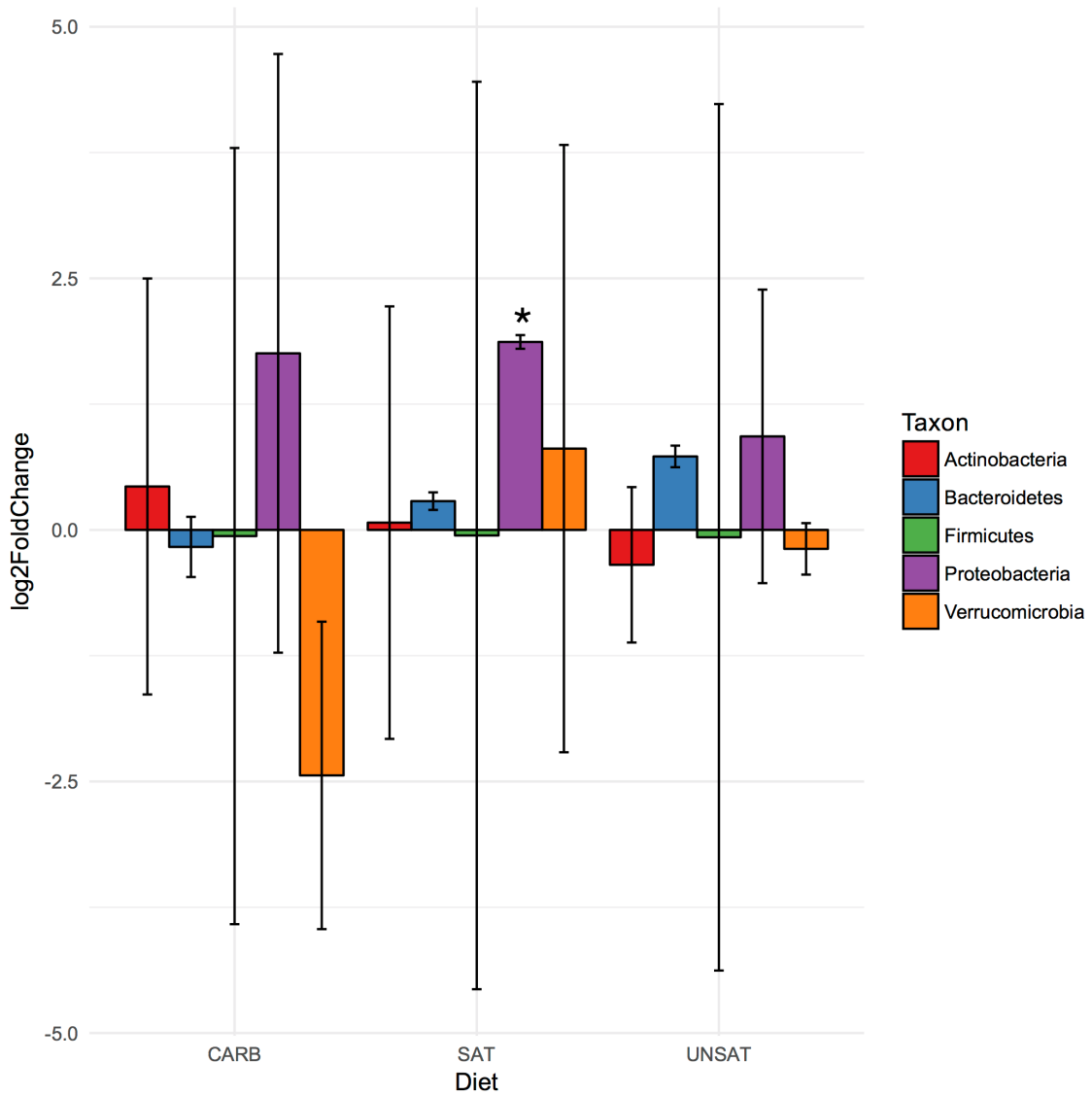
SUPPLEMENTARY DATA

Supplementary Figure S5. Microbiota composition in the study subjects at baseline.



SUPPLEMENTARY DATA

Supplementary Figure S6. Mean log₂ fold-changes (± standard error) of the bacterial phyla in the groups. The fold-changes and their statistical significance before and after overfeeding are based on negative binomial models. Significant difference is indicated by the asterisk (p<0.05).



SUPPLEMENTARY DATA

Supplementary Table S1. Dietary profiles of the groups before and after the overfeeding based on food records.

	SAT (n=14)		UNSAT (n=12)		CARB (n=12)	
	Before	After	Before	After	Before	After
Energy intake (MJ/day)	7.61 (6.02 – 9.18)	11.67 (9.87 – 13.41)*	8.88 (7.99 – 10.89)	12.07 (11.05 – 13.54)*	8.20 (7.36 – 10.49)	12.15 (11.14 – 15.79)*
Protein intake (E%)	19.8 (15.2 – 21.7)	15.0 (11.5 – 15.5)*	18.8 (16.2 – 20.9)	13.2 (11.9 – 15.3)*	19.5 (16.1 – 22.0)	11.4 (9.4 – 14.5)*
Carbohydrate intake (E%)	38.4 (32.2 – 41.3)	25.9 (23.0 – 32.2)*	34.5 (31.6 – 39.7)	22.7 (19.3 – 28.9)*	40.0 (36.9 – 47.8)	63.7 (58.1 – 67.5)*
Fat intake (E%)	39.4 (36.5 – 42.1)	58.9 (53.1 – 61.1)*	38.8 (32.0 – 43.5)	59.7 (53.6 – 63.6)*	35.6 (31.5 – 42.4)	23.8 (19.6 – 25.8)*
Saturated fat intake (E%)	12.9 (11.7 – 14.6)	32.7 (27.6 – 35.5)*	12.9 (11.0 – 16.0)	14.3 (13.5 – 18.3)	13.1 (11.7 – 15.2)	8.3 (6.5 – 9.7)*
Monounsaturated fat intake (E%)	13.9 (11.9 – 16.8)	12.8 (11.9 – 14.9)	13.2 (11.2 – 15.9)	27.7 (23.1 – 30.4)*	12.1 (10.8 – 14.4)	8.5 (6.4 – 9.4)*
Polyunsaturated fat intake (E%)	6.7 (6.4 – 8.5)	4.5 (4.0 – 5.2)*	5.1 (4.9 – 9.2)	11.4 (9.5 – 13.5)*	5.6 (5.1 – 7.0)	3.4 (3.2 – 4.0)*

Data are in median (25th-75th percentile). No differences between groups at baseline (Kruskal-Wallis test). * p<0.05 in Wilcoxon Signed Rank test between Before and After within a group.

SUPPLEMENTARY DATA

Supplementary Table S2. Baseline fatty acid compositions of VLDL-TG according to groups.

Total	SAT (n=14)	UNSAT (n=12)	CARB (n=12)
C14:0 (%)	1.8 ± 0.2	2.0 ± 0.2	2.3 ± 0.2
C16:0 (%)	26.2 ± 1.0	27.0 ± 0.9	27.8 ± 0.8
C16:1 n-7 (%)	4.6 ± 0.5	4.4 ± 0.3	5.2 ± 0.5
C18:0 (%)	3.1 ± 0.3	3.3 ± 0.3	3.1 ± 0.3
C18:1 n-9 (%)	37.6 ± 0.9	37.8 ± 0.9	36.9 ± 0.9
C18:2 n-6 (%)	14.8 ± 1.0	13.7 ± 0.7	13.0 ± 0.9

Data are in means ± SEM. There were no significant differences in any variable between the groups.

SUPPLEMENTARY DATA

Supplementary Table S3. Plasma ceramide concentrations before and after overfeeding in the groups.

Lipid name	SAT			UNSAT			CARB		
	Mean Before	Mean After	Q value	Mean Before	Mean After	Q value	Mean Before	Mean After	Q value
Cer(d16:2(4E,6E)/22:1(13Z)(2OH))	6.78643	9.11274	0.36	7.71353	9.27031	0.96	9.89585	9.68906	0.74
	+/-	+/-		+/-	+/-		+/-		
Cer(d18:0/24:0)	0.96342	1.33409	0.0052	0.87035	1.25029	0.97	1.71856	1.3074	0.88
	4.10406	6.50034		+/-	+/-		+/-	+/-	
Cer(d18:0/h24:0)	0.38621	0.57013	0.011	0.48144	0.47258	0.99	0.48002	0.52112	0.72
	1.06967	1.56036		+/-	+/-		+/-	+/-	
Cer(d18:0/h26:0)	0.06491	0.09943	0.59	0.08729	0.103	0.99	0.10395	0.17257	0.98
	0.76885	0.88989		+/-	+/-		+/-	+/-	
Cer(d18:1/24:0)	0.0358	0.09756	0.046	0.04429	0.07748	1	0.05797	0.09246	0.59
	2.84316	4.15985		+/-	+/-		+/-	+/-	
Cer(d18:1/24:1(15Z))	0.31666	0.34251	0.0026	0.35171	0.39869	0.96	0.40393	0.48568	0.59
	1.07751	1.54825		+/-	+/-		+/-	+/-	
Cer(d18:1/26:0)	0.10154	0.14089	0.53	0.11128	0.13142	0.97	0.13407	0.11646	0.72
	2.07704	3.1566		+/-	+/-		+/-	+/-	
Cer(d18:1/26:1(17Z))	0.17362	0.33601	0.29	0.2555	0.33441	0.97	0.14202	0.18681	0.7
	0.45668	0.59172		+/-	+/-		+/-	+/-	
Cer(d18:2/23:0)	0.02678	0.07791	0.0076	0.03213	0.05571	0.99	0.04149	0.04814	0.83
	0.86491	1.31764		+/-	+/-		+/-	+/-	
Cer(m18:0/24:0)	0.10664	0.09732	0.0018	0.10233	0.12264	0.99	0.18622	0.1233	0.93
	1.28955	2.09629		+/-	+/-		+/-	+/-	
Cer(m18:1(4E)/24:0)	0.18757	0.21783	0.034	0.24432	0.20338	0.99	0.14476	0.17573	0.92
	1.02325	1.60998		+/-	+/-		+/-	+/-	
Cer(m18:1(4E)/24:1(15Z))	0.12517	0.1801	0.011	0.22107	0.20404	0.97	0.1927	0.19509	0.7
	1.96867	2.60291		+/-	+/-		+/-	+/-	
Cer(m18:1(4E)/26:1(17Z))	0.13806	0.17806	0.02	0.21621	0.16879	0.97	0.46321	0.2227	0.72
	2.69515	4.29115		+/-	+/-		+/-	+/-	
	0.29105	0.37047		0.42431	0.42823		0.24066	0.29993	